The EMBO Journal vol.13 no.24 pp.5810–5817, 1994

Crystal structure of AmiC: the controller of transcription antitermination in the amidase operon of *Pseudomonas aeruginosa*

Laurence Pearl[1], Bernard O'Hara, Robert Drew and Stuart Wilson

Biomolecular Structure Group, Department of Biochemistry and Molecular Biology, University College London, Gower Street, London WC1E 6BT, UK

[1]Corresponding author

Communicated by T.Blundell

The crystal structure for the negative regulator (AmiC) of the amidase operon from *Pseudomonas aeruginosa* has been solved at a resolution of 2.1 Å. AmiC is the amide sensor protein in the amidase operon and regulates the activity of the transcription antitermination factor AmiR, which in turn regulates amidase expression. The AmiC structure consists of two domains with an alternating β−α−β topology. The two domains are separated by a central cleft and the amide binding site is positioned in this cleft at the interface of the domains. The overall fold for AmiC is extremely similar to that for the leucine−isoleucine−valine binding protein (LivJ) of *Escherichia coli* despite only 17% sequence identity, however, the two domains of AmiC are substantially closed compared with LivJ. The closed structure of AmiC is stabilized significantly by the bound acetamide, suggesting a molecular mechanism for the process of amide induction. The amide binding site is extremely specific for acetamide and would not allow a closed conformation in the presence of the anti-inducer molecule butyramide.

Key words: cytoplasmic receptor/gene regulation/ligand binding/periplasmic binding proteins/structural homology

Introduction

Pseudomonas aeruginosa is a pathogenic Gram-negative bacterium infecting burns and other surface wounds, and is responsible for the chronic lung infections which are the major cause of death in cystic fibrosis. *Pseudomonas aeruginosa* is capable of utilizing a very broad range of organic compounds as food sources, due to its possession of a large number of catabolic enzymes. One of these, the amidase enzyme, enables *P.aeruginosa* to utilize simple aliphatic amides such as acetamide and propionamide as sole carbon and nitrogen sources, by hydrolysing these to ammonia and a carboxylic acid (Kelly and Clarke, 1962). Expression of the amidase enzyme is induced by the presence of amides, via an unusual signal transduction pathway.

The amidase enzyme is encoded by the *amiE* gene, which is the first open reading frame in a gene cluster *amiEBCRS* (Drew and Wilson, 1992) (Figure 1). Upstream of the *amiE* open reading frame, transcription is initiated at a constitutive promoter, but is terminated prematurely after only 100 bases, 30 bases before the start codon of *amiE*, at a rho-independent transcription terminator (Drew and Lowe, 1989). Transcription past this point requires the product of the *amiR* gene, which is believed to prevent the formation of the terminator secondary structure. The antitermination activity of the AmiR protein is insensitive to the presence or absence of amides, and systems consisting of the *amiE* and *amiR* genes alone, express amidase enzyme constitutively (Wilson *et al.*, 1993). Sensitivity to amides is conferred by the *amiC* gene whose product inhibits the antitermination activity of AmiR in the absence of amides. Wild-type inducible amidase expression can be reconstructed *in vivo* by the presence of the *amiE*, *amiC* and *amiR* genes alone. The derived amino acid sequences of the *amiB* and *amiS* genes, which are not involved in regulation of expression, suggest that they are components of an ABC transporter system (Drew and Wilson, 1992).

The AmiC protein, the signal transducer controlling the expression of amidase in response to amides, is a dimer of

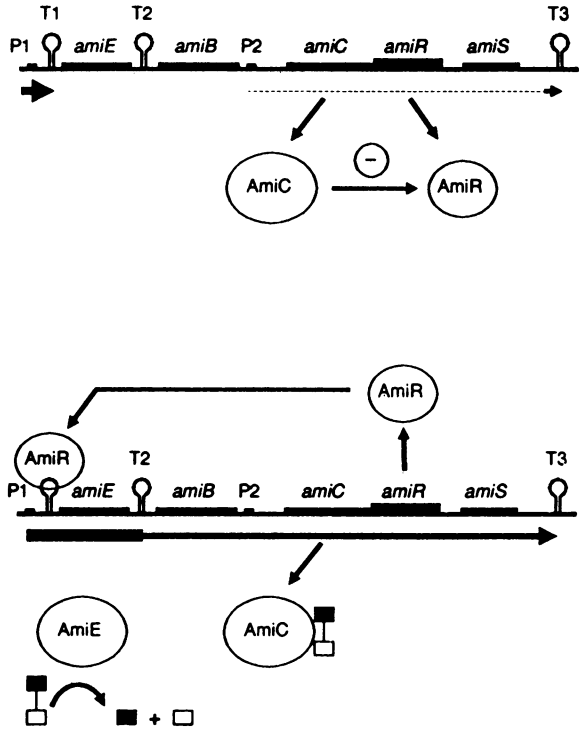

Fig. 1. Genetic organization and control of the amidase operon. (**a**) In the uninduced state, AmiC inhibits AmiR and transcription of the *amiE* gene is prematurely terminated by formation of a stem−loop structure (T1) in the nascent mRNA, between the promoter (P1) and the start of the *amiE* structural gene. (**b**) Binding of amide inducers (linked boxes) to AmiC relieves inhibition of AmiR which prevents termination at the stem−loop and allows transcription of the whole operon. A weak promoter (P2) provides a low level of transcription of the *amiC*, *amiR* and *amiS* genes in the uninduced state.

Table I. Data collection statistics

Data set	λ (Å)	d_{min} (Å)	N unique	% Complete	Multiplicity	R_{merge}
Native-1	0.870	2.5	11850	90	4.2	0.041
Native-2	0.9199	3.0	6355	93	3.7	0.032
Native-3	0.882	2.1	19614	91	4.4	0.064
Combined	–	2.1	21687	96	–	0.101
HgAc-1	1.5418	2.4	14042	93	3.0	0.036
HgAc-2	1.5418	3.0	6613	86	3.9	0.054
HgAc-LII	0.8363	2.5	13115	98	6.0	0.045

Data collection statistics. λ, X-ray wavelength used for data collection. N unique, number of unique reflections after data reduction. % complete, fraction of possible reflections actually measured. Multiplicity: total number of observations/number of symmetry unique reflections.
R_{merge}, $\Sigma\Sigma_i \mid I(h)-I(h)_i \mid / \Sigma\Sigma_i I(h)$ where $I(h)$ is the mean intensity after rejection of outliers. d_{min}, spacing of highest angle diffraction data. The R_{merge} for the combined data is for 6154 common reflections between the Native-2 and Native-3 data sets.

Table II. Heavy-atom refinement and phasing statistics

Derivative	No. of sites	d_{phase} (Å)	<Δiso>	R_{Cullis} cent,acent	Phasing power cent,acent
HgAc-1	6	2.5	0.24	0.66, 0.51	1.5, 2.7
HgAc-2	5	3.0	0.29	0.66, 0.56	1.4, 2.3
HgAc-L_{II}	6	2.5	0.29	0.71, 0.59	1.2, 2.2

<Δiso>, mean isomorphous difference $\Sigma| |F_{PH}|-|F_P| | / |F_P|$
R_{Cullis}, $\Sigma| |F_{PH}-F_P|-|F_H| | / |F_{PH}-F_P|$
Phasing power, $\Sigma|F_H| / \Sigma (| |F_P|e^{(i\theta)} + F_H|-|F_{PH}|)$
where $|F_{PH}|$ and $|F_P|$ are the observed derivative and native amplitudes, F_H is the calculated heavy atom structure factor, and θ is the calculated phase angle. Summations are over all observations. 'cent' and 'acent' refer to values for the centric and acentric reflections.

43 kDa monomer molecular weight, and binds acetamide *in vitro*, with a K_D of 3.5 μM (Wilson *et al.*, 1993). The AmiR protein, the transcription antitermination factor, appears to be a dimer of 21 kDa monomer molecular weight, which binds specifically to the 5′-end of the *amiE* mRNA (unpublished observations). AmiC has been shown to regulate the action of AmiR by a protein–protein interaction *in vivo* and preliminary results suggest that AmiC binds AmiR *in vitro*. In order to gain further insight into the functioning of this unusual genetic regulatory system, we have cloned the *amiC* and *amiR* genes, and overexpressed, purified and crystallized the AmiC protein (Wilson *et al.*, 1991). In this paper we report the determination of the crystal structure of AmiC at a resolution of 2.1 Å.

Table III. Refinement statistics

No. of protein atoms (non-hydrogen)	2919
No. of ligand atoms	4
No. of water molecules	127
R-factor	0.192 [$I>2\sigma(I)$]
	0.206 (all data)
R-free	0.275
R.m.s. deviation in bond lengths	0.019 Å
R.m.s. deviation in bond angles	2.2°
R.m.s. deviation in improper torsions	1.8°

R-factors are for 20 075 reflections [$I>2\sigma(I)$] and 20 650 reflections (all data) in the resolution range 8–2.1 Å. The free *R*-factor (Brunger, 1992b) was calculated from a random selection of 1015 reflections, constituting ~5% of the data with $I>2\sigma(I)$. R.m.s. deviations are from ideal values derived from Engh and Huber (1991).

Results

The crystal structure of AmiC was determined by isomorphous replacement with a single mercury acetate derivative, using isomorphous difference and anomalous scattering data collected at two different X-ray wavelengths. (Details of data collection, data processing, phasing, structure determination, model building and refinement, are given in Materials and methods. Crystallographic statistics are given in Tables I–III.)

Overall structure of AmiC

The AmiC structure consists of two distinct domains each with an alternating α/β topology. The domain containing the N-terminus (N-domain) consists of five parallel β-strands forming a highly twisted β-sheet flanked on both faces by α-helices. The other domain (C-domain) has a similar topology, with a central core of four parallel β-sheets flanked by helices, but with an additional β-hairpin anti-parallel to the edge of the central sheet. The polypeptide chain crosses over three times between the two domains, which come close together to form an extensive interface (Figure 2). The AmiC fold is extremely reminiscent of the doubly wound β–α–β topology found classically in the periplasmic binding protein family (Quiocho, 1991) and in proteins of such disparate function as transferrin (Bailey *et al.*, 1988) and porphobilinogen deaminase (Louie *et al.*, 1992). This possibility for the AmiC structure had been suggested in earlier work on the basis of secondary structure prediction and optimal sequence threading (Wilson *et al.*, 1993), although the highest observed sequence homology to any of these proteins is <20% identity. Closer comparison with one of these β–α–β proteins, the leucine–isoleucine–valine binding protein of *Escherichia coli* (LivJ, Brookhaven Protein Databank entry P2LIV) reveals a remarkable degree of structural similarity. Taken separately, the two

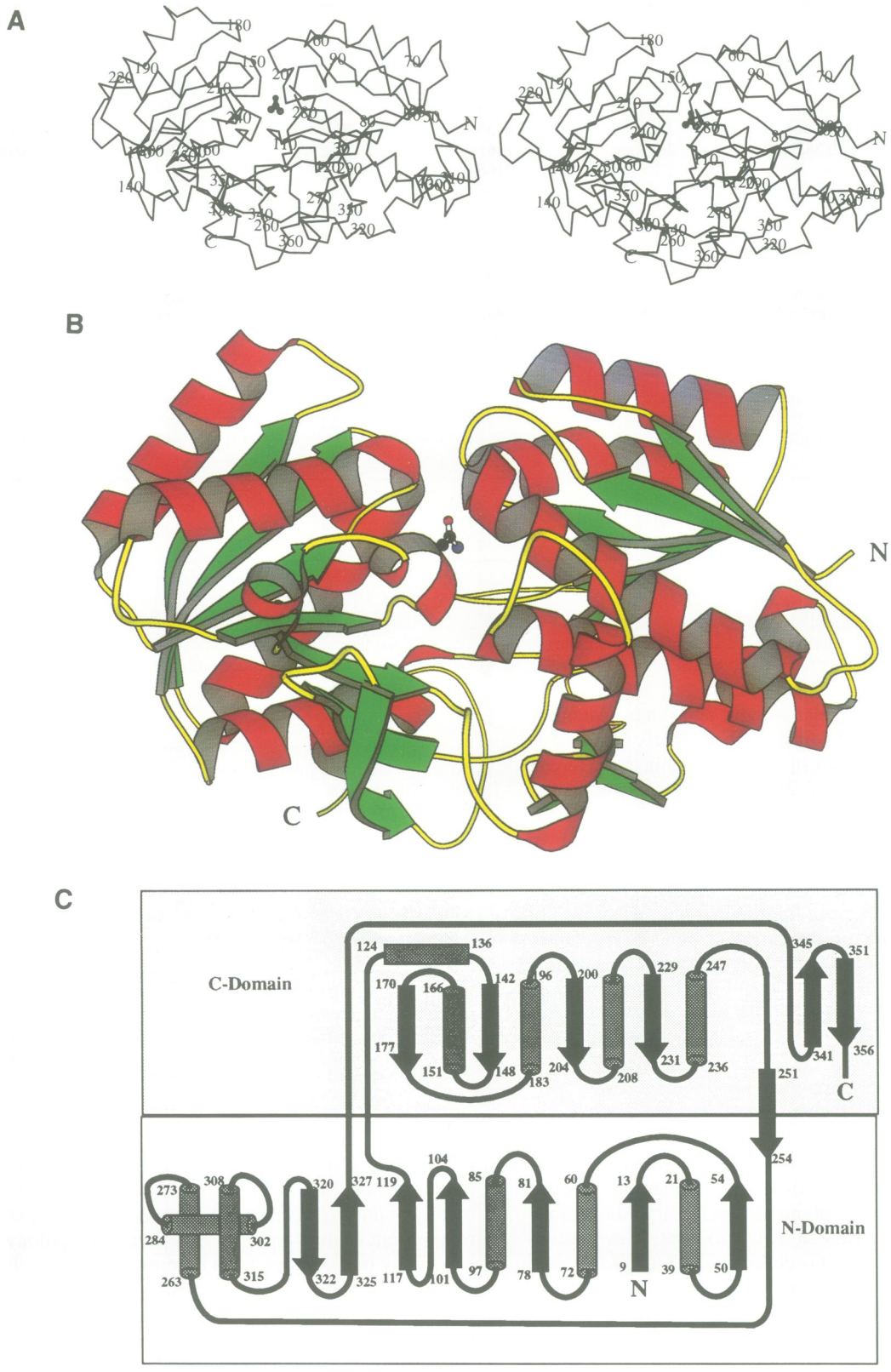

Fig. 2. Structure of AmiC. (**A**) Stereo Cα-trace of AmiC. The N- and C-termini are indicated, and every 10th residue is labelled. The bound acetamide is shown as a ball-and-stick molecule, with oxygen coloured red, nitrogen blue and carbon black. (**B**) Secondary structure cartoon of AmiC.The N-domain is on the right, the C-domain on the left. α-helices are coloured red, β-strands green, and coils and loops yellow. The bound acetamide molecule lies between the two domains. The figure was generated using MOLSCRIPT (Kraulis, 1991). The view is the same as (A). (**C**) Secondary structure of AmiC. Helices are drawn as cylinders, sheets as broad arrows.

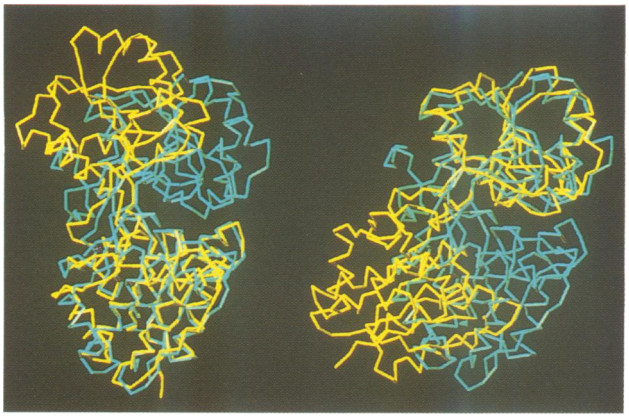

Fig. 3. Comparison of AmiC and LivJ. AmiC (blue) superimposed on LivJ (yellow) by matching the N-domain, (left picture) and by matching the C-domain (right picture). The figure was generated using O (Jones *et al.*, 1991). The view is rotated by 90° relative to Figure 2.

domains of AmiC can be superimposed on the corresponding domains of LivJ with root mean square deviations of 1.45 Å between 116 common Cα positions for the N-domains and 1.76 Å for 124 common Cα positions in the C-domains. The relative orientation of the two domains differs considerably between the two proteins; in LivJ the two domains are opened up and make few mutual contacts, whereas in AmiC the two domains are tightly juxtaposed and form an extensive interface in the middle of the protein. To superimpose both domains of AmiC with the corresponding domains in LivJ simultaneously, requires a hinge rotation of some 35° (Figure 3).

AmiC is longer than LivJ by three residues at the N-terminus and by 30 residues at the C-terminus. The C-terminal extension consists of a proline-rich coil and a short helical segment which underlie the inter-domain strands, on the opposite side of the molecule to the domain interface. The first six residues at the N-terminus and the last nine residues of the C-terminal extension, of which three are glycine, cannot be located in the electron density and are presumed to be disordered. The disulfide bond between cysteines 53 and 78 in LivJ, does not occur in AmiC, in accordance with its cytoplasmic location, the corresponding residues becoming Gly and Met respectively. A 'forbidden' backbone conformation found in LivJ at His76 (ϕ = 82°, ψ = 123°) is also found in AmiC at the corresponding residue, Cys82 (ϕ = 83°, ψ = 139°).

The AmiC protein purified from an overexpressing *P.aeruginosa* clone, migrates as a dimer in gel filtration, but crystallizes in $P4_22_12$ with a monomer in the asymmetric unit. The degree of interaction in the crystal between the monomer at *x*, *y*, *z* and the symmetry related monomer at *y*, *x*, $-z$ is by far the most extensive and suggests that this pair of molecules constitute the biological dimer (Figure 4). The dimer is mainly held together by a network of hydrogen bonding and salt bridge interactions involving the side chains of His158, Arg161 and His370 from one monomer, with the side chain of Glu96 and main chain of Arg331 and Tyr113 on the other. Towards the centre of the dimer interface, the side chains of Tyr366 from each monomer are in mutual van der Waals contact and each makes a hydrogen bond with the peptide oxygen of Glu112 on the other monomer.

Ligand binding site

The biological role of AmiC is to act as a 'sensor' for amides and to trigger expression of the amidase operon when amides are present in the environment of the bacterium. In the archetypal *P.aeruginosa ami*$^+$ strain PAC1 (Kelly and Clarke, 1962), amidase expression is strongly induced by acetamide and propionamide, and by lactamide and various N-substituted amides, however, equilibrium dialysis studies indicate that acetamide and propionamide bind at least 100-fold more tightly to AmiC *in vitro* than these other amides (Wilson *et al.*, 1993). That amides such as lactamide and N-substituted amides are relatively good biological inducers of the amidase operon *in vivo*, despite their weak binding to AmiC *in vitro*, is the result of their resistance to hydrolysis by the amidase whose expression they induce. In contrast, acetamide binds tightly to AmiC, but is rapidly hydrolysed by the amidase *in vivo*. Butyramide, which binds weakly to AmiC *in vitro*, is a competitive inhibitor of induction *in vivo*.

Crystals of AmiC have been grown with a variety of amides, (acetamide, lactamide and butyramide), added to the crystallization mixture. Crystals grown in all these conditions, and in the absence of added amide, show a peak of electron density, of similar appearance, at the interface between the two domains. This peak is present in all electron density maps ranging from the first density modified isomorphous replacement phased map at 3.0 Å, to σ_A weighted $2|F_o|-|F_c|$ maps (Read, 1986) at 2.1 Å resolution with phases derived from the refined protein coordinates only (Figure 5). This peak lies within a pocket formed at the interface of the two domains, with Ser85 from the N-domain forming the top, and Thr233 from the C-domain forming the bottom. The walls of the pocket are formed by Tyr83, Tyr104, Thr106 and Pro107 from the N-domain and Tyr150, Tyr152 and Val206 from the C-domain. This location in the AmiC structure is very similar to the position at which ligands have been observed to bind in the periplasmic binding proteins in general (Quiocho, 1991) and the LivJ protein in particular (Sack*s* *et al.*, 1989). The nucleotide sequence (unpublished data) of a phenotypic variant, PAC181, which is inducible by butyramide (Turberville and Clarke, 1981), shows a Thr→Asn mutation at residue 106, one of the groups lining the pocket. It seems probable that this pocket represents the ligand binding site and that the electron density observed here is due to a bound ligand.

It had been assumed previously that AmiC purified from an over-producing clone grown without explicitly added amide, would be essentially ligand-free. The presence of clear electron density for a bound ligand, even when no amide was added to the crystallization mixture, suggests that this assumption was incorrect. The appearance of the ligand peak is extremely similar between crystals grown with acetamide, butyramide, DL-lactamide or no amide added to the crystallization mixture. The size and shape of the electron density peak and its environment are consistent with acetamide, which has the highest affinity for binding to AmiC (Wilson *et al.*, 1993), and is the amidase enzyme's preferred substrate (Kelly and

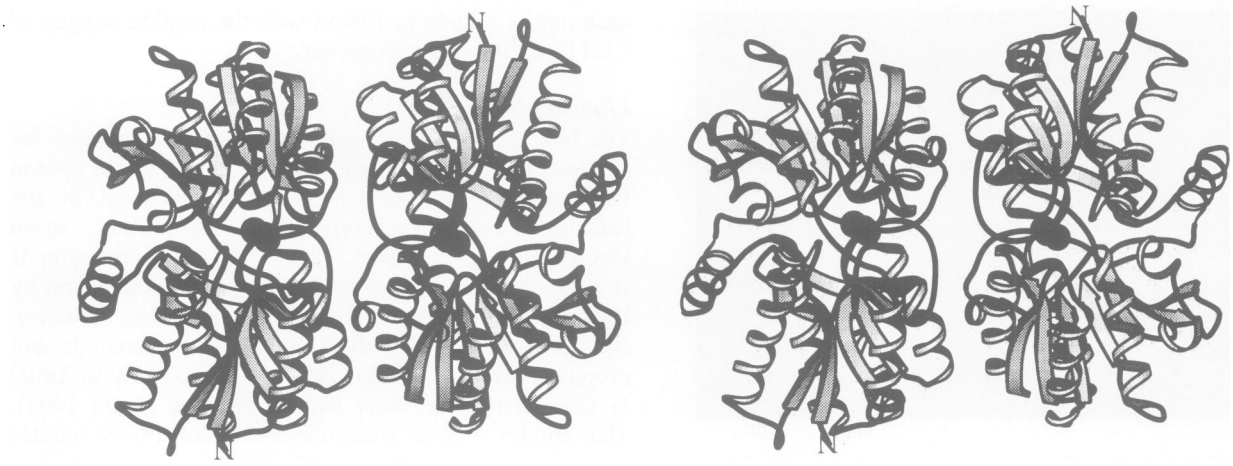

Fig. 4. AmiC dimer. Probable biological dimer of AmiC. Although AmiC is a dimer in free solution, there is only a single molecule in the asymmetric unit, and the dimer is generated by a crystallographic 2-fold axis. The acetamide molecule is shown as a space-filling model.

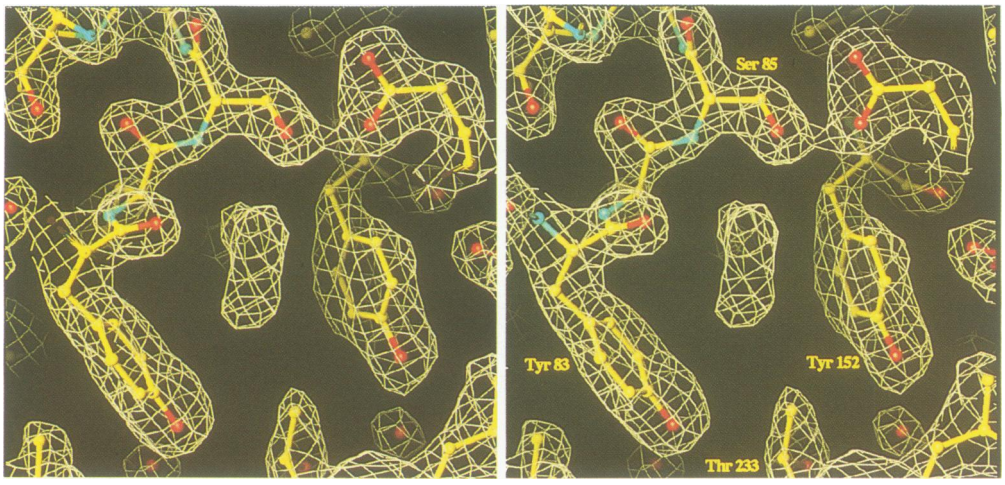

Fig. 5. Amide electron density. Stereo view of the electron density for the acetamide ligand in the binding pocket. The electron density map was calculated with coefficients $2|F_o|-|F_c|$, and phases from the refined protein and solvent atoms with the acetamide molecule omitted. Contours are at 1.5× r.m.s. of the electron density. The figure was generated using O (Jones *et al.*, 1991).

Clarke, 1962). In addition, *in vitro* AmiC–AmiR binding data indicate that purified AmiC behaves identically to AmiC which has been dialysed extensively against acetamide (unpublished observations). In crystals grown in the presence of additional acetamide, which would be expected to displace any other endogenous ligand, the electron density in this region is identical to crystals grown with other amides or with no added amide. It appears likely that AmiC is binding acetamide either produced by the metabolism of the bacterium, or more probably, present in the complex organic mixture used to prepare the bacterial growth medium. Although acetamide is not expected to be a significant component of the bacterial growth medium, a concentration of much less than micromolar would be more than sufficient to saturate all the AmiC present in the bacterial cells. With acetamide bound, the concentrations of the larger amides, lactamide and butyramide used in some crystallization experiments would have been much too low to compete with the much tighter binding ligand, acetamide. Periplasmic binding proteins are often found to co-purify with their preferred ligand bound; given its structural similarity to these proteins, it is not surprising that AmiC should do likewise.

An acetamide molecule modelled into the observed electron density of the refined protein structure makes an extensive set of hydrogen bonding and van der Waals contacts with groups in the domain interface and, when included in crystallographic refinement, refines with low temperature factors, indicative of a highly occupied, tightly bound ligand. The amide oxygen accepts hydrogen bonds from the peptide nitrogen of Ser85 and the phenolic hydroxyl of Tyr150, and the amide nitrogen makes hydrogen bonding contacts with the side chain hydroxyl of Ser85 and the main chain carbonyl oxygen of Pro107. The amide nitrogen makes a third contact of hydrogen bonding distance with the phenolic hydroxyl of Tyr104, however, this is directed perpendicular to the plane of the amide and may involve an interaction with the amide nitrogen lone pair. The hydrogen bonds to the peptide nitrogen of Ser85 and to the peptide oxygen of Pro107 serve to define the orientation of the amide group unambiguously. The plane of the acetamide molecule is packed against the plane of the phenol ring of Tyr152 on one face of the pocket, while the methyl group is in van der Waals contact with the side chain of Tyr83 on the opposite face, and the side chain methyl of Thr233 at the base of the pocket (Figure 6).

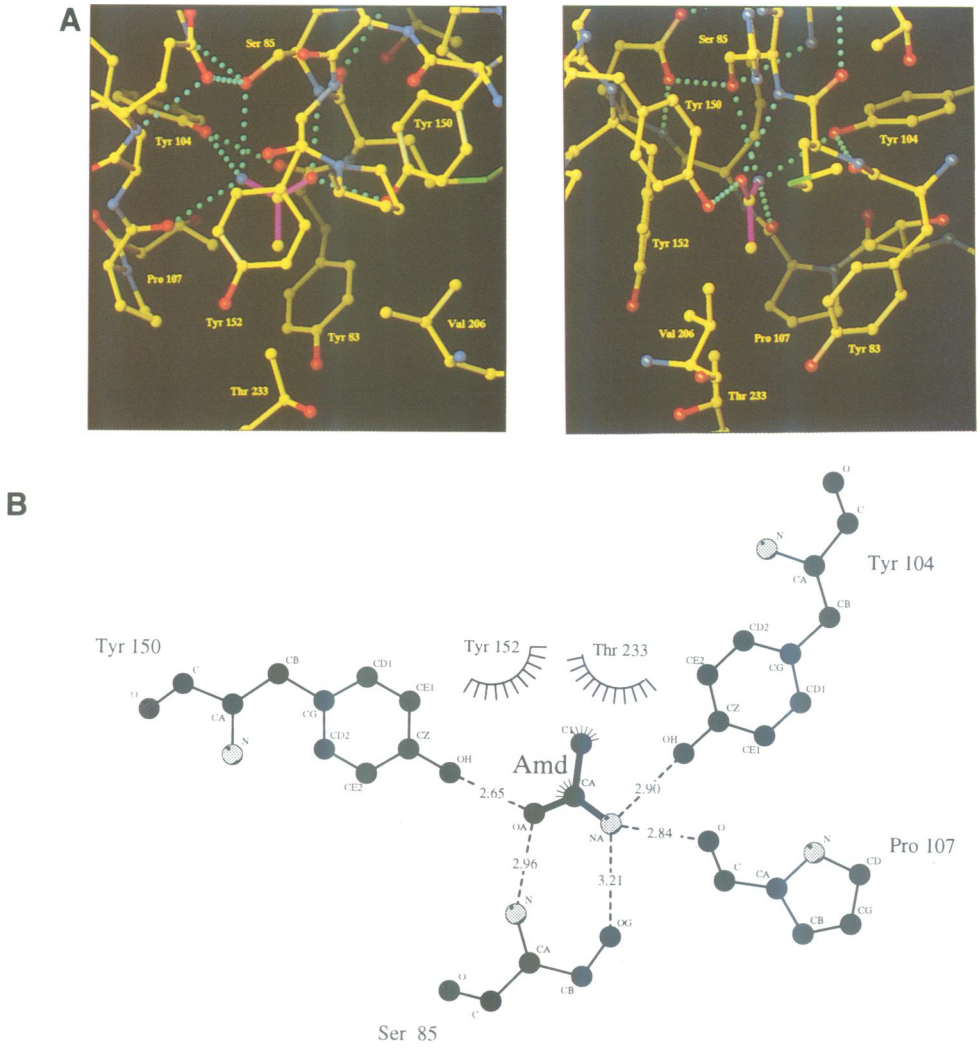

Fig. 6. Interactions in the amide binding site. (**a**) Two perpendicular views of the refined structure including acetamide. Hydrogen bonding contacts are indicated by the lines of blue spheres. See the text for a detailed description.The figure was generated using O (Jones *et al.*, 1991). The bonds in the acetamide molecule are highlighted in magenta. Oxygen atoms are shown as red spheres, nitrogen as blue spheres and carbon as yellow spheres. The view in (a) is approximately perpendicular to Figure 5, while the view in (b) is rotated by ~180 degrees. (**b**) Schematic diagram of the hydrogen bonding and van der Waals interactions of the bound acetamide. The figure was generated by the program Ligplot (A.C.Wallace and R.A.Laskowski, personal communication).

Discussion

Similarity to periplasmic binding proteins

The AmiC structure shows remarkable similarity to the structures of group-II bacterial periplasmic binding proteins in general, and to branched-chain amino acid binding proteins such as LivJ in particular, although their amino acid sequence identity with any of these proteins is <20% (Wilson *et al.*, 1993). Although the position of the ligand binding site is conserved between AmiC and LivJ, the residues comprising the binding site are not, reflecting the difference in their preferred ligands. In particular the loop connecting the fourth and fifth strands in the N-domain is three residues shorter in AmiC. A detailed comparison of the AmiC and LivJ ligand binding sites will be presented elsewhere.

The structures of the corresponding domains of AmiC and LivJ are very similar, however, their relative juxtaposition is very different. In the AmiC structure, the interactions with the amide ligand come from groups in both domains. LivJ, crystallized in the absence of ligand, shows an open conformation with little contact between the faces of the domains. That the structure of the LivJ–leucine complex is also in an open conformation is probably not significant, as this complex was formed by soaking existing ligand-free LivJ crystals in leucine (Sacks *et al.*, 1989). The closed conformation observed in the ligand-bound AmiC structure and the open conformation observed in the ligand-free LivJ indicates the considerable conformational flexibility available to this fold.

On the basis of their structural similarity, AmiC and LivJ probably share a common ancestor. The detailed molecular function of the two proteins is also extremely similar. Both are highly specific binding proteins for small molecule ligands, and both are involved in ligand dependent interactions with a second protein. It is the biological roles that the two proteins play which are radically different. LivJ acts as a scavenging receptor in the periplasmic space of the bacterium, delivering its ligand to the outer face of an ATP-dependent translocation system, a role it shares with many other well described

homologues (Quiocho, 1991). AmiC serves as a cytoplasmic receptor/transducer, controlling the activity of a second cytoplasmic protein directly involved in the regulation of gene expression. This biological role for a member of this structural family is so far unique.

Structural basis of amide induction specificity of the amidase operon

The amidase system was originally identified and selected for its ability to be induced by and to utilize acetamide. It is not surprising therefore that the ligand binding site in AmiC, the amide 'sensor' in the amidase operon, is perfectly adapted to the binding of acetamide. Interactions between acetamide and the protein are divided between residues in the two domains. The majority of the contacts with the amide group and two walls of the hydrophobic pocket are from the N-domain, whilst the C-domain provides the other two walls and the 'lid' of the pocket, and the second hydrogen bond to the amide oxygen. The bound ligand, which is completely buried in the domain interface, functions as a 'pin', linking the two halves of the binding pocket. Periplasmic binding proteins are believed to undergo conformational change on ligand binding, changing from an 'open' conformation to a closed conformation entrapping the ligand at the domain interface (Quiocho, 1991). As AmiC is clearly a member of this structural family, it is not unreasonable to propose that it functions in a similar fashion. We suggest that AmiC, in the absence of ligand, is in a more 'open' conformation, similar to that seen for LivJ. Ligand binding would serve to stabilize the 'closed' conformation observed in AmiC crystals, by making simultaneous contacts with the faces of both domains.

Whether an amide binding to the N-domain half of the pocket will stabilize the closed or the open conformation of the domains, will depend on the size of the alkyl chain attached to the amide group. A short chain as in acetamide or lactamide will simultaneously permit the van der Waals interactions between the side chain of Thr233 and the amide alkyl chain, and between the side chain of Tyr152 and the amide face, and the hydrogen bond between Tyr150 and the amide carbonyl oxygen, which form one half of the pocket and together stabilize the closed conformation. A larger alkyl chain as in butyramide would severely obstruct the packing of the side chain of Thr233, prevent formation of the pocket and de-stabilize the closed conformation. The observed binding affinities and the biological effects of different amides on induction of the amidase operon are simply rationalized by this structural model. Acetamide and propionamide, the strongest AmiC ligands, are potent inducers of amidase expression. Amides with slightly bulkier alkyl chains such as lactamide, which would still allow a reasonably closed conformation, are also inducers. Butyramide, with a still longer alkyl chain, is a competitive inhibitor of induction and, although able to form the N-domain interactions, would prevent closure of the pocket and thus de-stabilize the closed conformation. Formamide which is also a competitive inhibitor of induction, would not sterically prevent closure but could not form the substantial hydrophobic interactions in the pocket which would stabilize the closed conformation. It is a necessary sequitur of this argument that the molecular mechanism of induction involves formation of the closed conformation.

The mechanism of AmiR regulation by AmiC

In the absence of inducing amides such as acetamide, AmiC inhibits transcription antitermination by AmiR (Wilson *et al.*, 1993). Although we have not yet observed the ligand-free conformation of AmiC crystallographically, it is reasonable to suppose, given their strong structural similarity, that it would possess an open conformation similar to that observed in the unliganded LivJ protein (Sacks *et al.*, 1989). Addition of acetamide would switch AmiC into the closed conformation observed in the structure presented here. Several studies have shown similar domain motions in solution for various periplasmic binding proteins (Newcomer *et al.*, 1981; Jacobsen *et al.*, 1991; Luck and Falk, 1991; Vermersch *et al.*, 1991),

In vivo data have shown that AmiC regulates AmiR via direct protein–protein interaction (Wilson *et al.*, 1993). A simple model might then be suggested in which AmiC, in the open conformation, binds to AmiR and thereby prevents its interaction with the nascent mRNA. Binding of acetamide would switch AmiC into the closed conformation which does not bind AmiR, thereby releasing it to function in antitermination. This model would be consistent with the observation that expression of amidase in an *in vivo* system consisting of the *amiE* and *amiR* genes alone is constitutive and insensitive to the action of amides. The system may however, be more complicated, as an AmiC–AmiR complex, formed *in vitro*, is stable to the presence of saturating concentrations of acetamide (unpublished observations). If AmiC does indeed bind AmiR in the presence of acetamide, then no simple association/dissociation model would be adequate to explain induction. Rather AmiC and AmiR must exist as a complex with AmiC as the regulatory component and AmiR as the 'effective' component, with the conformational change elicited in AmiC on binding acetamide causing a concomitant change in the conformation of AmiR to an active form or a rearrangement of the AmiC–AmiR complex.

The structure of AmiC with a bound ligand, presented here, suggests a molecular mechanism for the first step in the process of induction in the amidase operon, but further work will be required to elucidate the means by which this initial signal is communicated to the AmiR protein, and how the AmiR protein itself acts in transcription antitermination.

Materials and methods

Protein production and crystallization

AmiC protein was purified from an over expressing plasmid in *P.aeruginosa*, and purified as described (Wilson *et al.*, 1991). Small crystals were grown essentially as described (Wilson *et al.*, 1991) and enlarged by macro-seeding in droplets containing AmiC 12 mg/ml, PEG 4000 6% (w/v), Tris–HCl 20 mM, pH 8.0 and $(NH_4)_2SO_4$ 150 mM, under paraffin oil in Terasaki dishes. Three different crystal habits have been observed in these conditions; Type-1 are tetragonal rods, Type-2 are thin plates, Type-3 are chunky prisms. Structure solution has centred on the Type-1 crystals, which diffract most strongly and are most reproducible. Type-1 crystals have space group $P4_22_12$. Small variations in the unit cell parameters have been observed between these crystals; most have unit cells with a = 105.4 Å, c = 66.6 Å and diffract to 2.5 Å, resolution, while some crystals have unit cells a = 104.9 Å, c =

65.8 Å, and diffract to 2.1 Å. Heavy-atom soaking was performed on crystals resuspended in a stabilizing solution of 11% PEG4000, 150 mM $(NH_4)_2SO_4$ and either 20 mM Tris−HCl (pH 8.0) or 20 mM Tris-acetate (pH 8.0), with 2 mM $Hg(CH_3COO)_2$.

Data collection and processing

Medium resolution native, and some derivative data were collected using CuKα radiation (λ = 1.5418 Å) on a MAR Research 18 cm Image Plate Detector at Birkbeck College. Medium and high resolution native data and some derivative data were collected using synchrotron radiation (λ = 0.8363, λ = 0.9199) at Station 9.5, Daresbury SRS on a MAR Research 18 cm Image Plate Detector, and using synchrotron radiation (λ = 0.882 Å) at Station 9.6, Daresbury SRS on a MAR Research 30 cm Image Plate detector. Diffraction images were integrated using the MOSFLM package (A.G.W.Leslie, LMB Cambridge) and reduced using the Rotavata/Agrovata and Truncate programs of the CCP4 Suite (CCP4, 1979). The Combined native data set used in refinement was a 2.1 Å resolution data set (collected at 0.882 Å) merged with a 3.0 Å data set (collected at 0.9199 Å) to provide low resolution data.

Heavy atom phasing

Data were collected from crystals soaked in mercury acetate buffered in Tris−HCl, with CuKα radiation and with synchrotron radiation tuned to the Hg L_{II} edge (0.8363 Å) for an optimized anomalous signal. Crystals were carefully mounted with c* along the spindle axis, and 2° oscillation angles used, to maximize the number of Freidel pairs measured on the same image. A third data set was collected with CuKα radiation from a crystal also soaked in mercury acetate but buffered with Tris-acetate. Heavy atom positions in the mercury acetate soaked crystals were determined by Patterson superposition using the SHELX-90 program (Sheldrick, 1991), by vector verification using the VECSUM program (I.J.Tickle, Birkbeck College) and by hand calculation. Double difference and cross-phase Fourier maps were calculated to locate all the sites. The crystals soaked in mercury acetate in Tris−HCl buffer (HgAc-1, HgAc-LII) both had six mercury atoms bound, while the crystal soaked in mercury acetate buffered with Tris-acetate had five sites. Heavy atom parameters were refined by maximum likelihood phased refinement (Otwinowski, 1991) using the CCP4 program MLPHARE. Wavelength dependent contribution was modelled by refinement of an anomalous occupancy for each site, in each data set. Phases from MLPHARE were improved by solvent flattening and histogram equalization using SQUASH (Cowtan, 1991). The correct hand of heavy atom constellation was determined by inspection of maps calculated with density-modified phases including full anomalous scattering data; the correct hand gave clear solvent boundaries. <FOM> for data from 10 to 2.5 Å resolution before density modification was 0.64 for acentric reflections and 0.77 for centric reflections.

Model building and refinement

Electron density maps were interpreted using O (Jones *et al.*, 1991). The initial atomic model was refined against data to 2.5 Å resolution from a crystal with cell dimensions of a = 105.4 Å, c = 66.6 Å (Native-1 in Table I). Subsequently, this model was refined against higher resolution data from crystals with cell dimensions a = 104.9 Å, c = 65.8 Å at 2.1 Å. Refinement employed simulated annealing and conjugate gradient refinement in X-PLOR (Brunger, 1992a) using the geometric restraints based on Engh and Huber (1991). Maps were calculated with coefficients $|F_o|-|F_c|$ and $2|F_o|-|F_c|$ and σ_A-weighted according to Read (1986) to minimize model bias, and they were used in repeated cycles of manual adjustment and for location of solvent molecules. The current model consists of 370 of the 382 residues predicted from the DNA sequence of the *amiC* gene (EMBL Database PAAMIR X13776) and N-terminal sequencing of the expressed protein. In addition, 115 solvent molecules making at least one geometrically reasonable hydrogen bond to the protein have also been located, and included in the final refinement. Main-chain electron density in $2|F_o|-|F_c|$ is continuous from residues 7 to 375 at 1.0× the r.m.s. value of the electron density. The geometric parameters of the model have been analysed with PROCHECK (Laskowski *et al.*, 1993) and are all inside or better than the expected deviations from ideality at 2.1 Å resolution. A single residue, Cys82, has main chain torsion angles within a 'forbidden' region of a Ramachandran plot, but is unambiguous in the electron density. A similar violation is observed for a residue in the topologically equivalent position in the LivJ protein, suggesting that this unfavourable conformation, occurring at the beginning of a loop involved in ligand binding, may have a functional role.

Acknowledgements

We are grateful to the Department of Crystallography at Birkbeck College, and the SERC Daresbury Laboratory for use of their X-ray diffraction equipment and technical assistance, and to our colleagues at UCL for their support, and assistance with synchrotron data-collection. We particularly acknowledge the contributions of Dr Andrew Hemmings and Dr Robert Drew at earlier stages of the project, and Dr David Jones and Dr Ian Tickle for much useful discussion. Coordinates will be submitted to the Brookhaven Protein Databank on publication. This work was supported by the SERC (crystallography) and the Wellcome Trust (molecular biology).

References

Bailey,S. *et al.* (1988) *Biochemistry*, **27**, 5804–5812.
Brunger,A.T. (1992a) *X-PLOR Version 3.1. A System for X-Ray Crystallography and NMR*. Yale University Press, New Haven, CT.
Brunger,A.T. (1992b) *Nature*, **255**, 472–474.
CCP4 (1979) *A Suite of Programs for Protein Crystallography*. The SERC (UK) Collaborative Computing Project No. 4, distributed from Daresbury Laboratory, Warrington, UK.
Cowtan,K. (1991) In Moras,D., Podjarny,A.D. and Thierry,J.C. (eds), *Crystallographic Computing*. Oxford University Press, Oxford, pp. 373–381.
Drew,R.E. and Lowe,N. (1989) *J. Gen. Microbiol.*, **135**, 817–823.
Drew,R.E. and Wilson,S.A. (1992) In Galli,E., Silver,S. and Witholt,E. (eds), *Pseudomonas Molecular Biology and Biotechnology*. American Society of Microbiology, Washington DC, pp. 768–796.
Engh,R.A. and Huber,R. (1991) *Acta Crystallogr. A*, **47**, 392–400.
Jacobsen,B.L., He,J.J., Vermersch,P.S., Lemon,D.D. and Quiocho,F.A. (1991) *J. Biol. Chem.*, **266**, 522–525.
Jones,T.A., Zou,J.-Y., Cowan,S.W. and Kjeldgaard,M. (1991) *Acta Crystallogr. A*, **47**, 110–119.
Kelly,M. and Clarke,P.H. (1962) *J. Gen. Microbiol.*, **27**, 305–316.
Kraulis,P.J. (1991) *J. Appl. Crystallogr.*, **24**, 946–950.
Laskowski,R.A., MacArthur,M.W., Moss,D.S. and Thornton,J.M. (1993) *J. Appl. Crystallogr.*, **26**, 283–290.
Louie,G.V., Brownlie,P.D., Lambert,R., Cooper,J.B., Blundell,T.L., Wood,S.P., Warren,M.J., Woodcock,S.C. and Jordan,P.M. (1992) *Nature*, **359**, 33–39.
Luck,L.A. and Falk,J.J. (1991) *Biochemistry*, **30**, 6484–6490.
Newcomer,M.E., Lewis,B.A. and Quiocho,F.A. (1981) *J. Biol. Chem.*, **256**, 13218–13222.
Otwinowski,Z. (1991) In *Isomorphous Replacement and Anomalous Scattering: Proceedings of the CCP4 Study Weekend*. SERC, Daresbury Laboratory, Warrington, UK, pp. 80–85.
Quiocho,F.A. (1991) *Curr. Opin. Struct. Biol.*, **1**, 922–933.
Read,R.J. (1986) *Acta Crystallogr. A*, **42**, 140–149.
Sacks,J.S., Saper,M.A. and Quiocho,F.A. (1989) *J. Mol. Biol.*, **206**, 171–191.
Sheldrick,G.M. (1991) In *Isomorphous Replacement and Anomalous Scattering: Proceedings of the CCP4 Study Weekend*. SERC Daresbury Laboratory, pp. 23–38.
Turberville,C. and Clarke,P.H. (1981) *FEMS Microbiol. Lett.*, **10**, 87–90.
Vermersch,P.S., Tesemer,J.J.G., Lemon,D.D. and Quiocho,F.A. (1991) *J. Biol. Chem.*, **265**, 16592–16603.
Wilson,S.A., Chayen,N.E., Hemmings,A.M., Drew,R.E. and Pearl,L.H. (1991) *J. Mol. Biol.*, **222**, 869–871.
Wilson,S.A., Wachira,S.J., Drew,R.E., Jones,D. and Pearl,L.H. (1993) *EMBO J.*, **12**, 3637–3642.

Received on June 21, 1994; revised on September 20, 1994